Eduardo Fernández-Tarrazo, Eduardo; Sánchez-Sanz, Mario; Sánchez, Antonio L.; Williams, Forman A. (2016). A multipurpose reduced chemical-kinetic mechanism for methanol combustion. *Combustion Theory and Modelling*, 20:4, 613-631.

DOI: https://doi.org/10.1080/13647830.2016.1162330

RESEARCH ARTICLE

A multipurpose reduced chemical-kinetic mechanism for methanol combustion

Eduardo Fernández-Tarrazo[a*], Mario Sánchez-Sanz[a], Antonio L. Sánchez[b],

Forman A. Williams[b]

[a]*Dept. Ingeniería Térmica y de Fluidos, Universidad Carlos III de Madrid, Leganés 28911, Spain*; [b]*Dept. Mechanical and Aerospace Engineering, University of California San Diego, La Jolla CA 92093-0411, USA*

(*v1.0 released July 2015*)

A multipurpose reduced chemical-kinetic mechanism for methanol combustion comprising 8 overall reactions and 11 reacting chemical species is presented. The development starts by investigating the minimum set of elementary reactions needed to describe methanol combustion with reasonable accuracy over a range of conditions of temperature, pressure, and composition of interest in combustion. Starting from a 27-step mechanism, previously tested and found to give accurate predictions of ignition processes for these conditions, it is determined that addition of 11 elementary reactions taken from its basis (San Diego) mechanism extends the validity of the description to premixed-flame propagation, strain-induced extinction of nonpremixed flames, and equilibrium composition and temperatures, giving results that compare favorably with experimental measurements and also with computations using the 247-step detailed San Diego mechanism involving 50 reactive species. Specifically, premixed-flame propagation velocities and extinction strain rates for nonpremixed counterflow flames calculated with the 38-step mechanism show departures from experimental measurements and detailed-chemistry computations that are roughly on the order of 10%, comparable with expected experimental uncertainties. Similar accuracy is found in comparisons of autoignition times over the range considered, except at very high temperatures, under which conditions the computations tend to overpredict induction times for all of the chemistry descriptions tested. From this 38-step mechanism the simplification is continued by introducing steady-state approximations for the intermediate species CH_3, CH_4, HCO, CH_3O, CH_2OH, and O, leading to an 8-step reduced mechanism that provides satisfactory accuracy for all conditions tested. The flame computations indicate that thermal diffusion has a negligible influence on methanol combustion in all cases considered and that a mixture-average species-transport model is sufficiently accurate for premixed and nonpremixed flames, whereas for the former an even simpler constant-Lewis-number description gives equally satisfactory results.

Keywords: methanol combustion, reduced chemistry, autoignition, deflagration, diffusion-flame extinction

1. Introduction

The global demand for methanol has increased steadily in recent decades because of its direct use as liquid fuel to power passenger cars [1] and its role as feedstock for the production of dimethyl ether, which was of interest as a potentially clean alternative to diesel fuel for trucks and buses [2]. Compared to normal gasoline, methanol has a lower energy density, resulting in the requirement of a larger fuel tank for the same vehicle range, but this drawback is partially offset by the

*Corresponding author. Email: eafernan@ing.uc3m.es

ISSN: 1364-7830 print/ISSN 1741-3559 online

DOI: 10.1080/13647830.YYYY.xxxxxx
http://www.tandfonline.com

higher efficiency of engines running with methanol [3]. Its efficient and economical production from different renewable sources, including biomass and CO_2, and its potential for integration into the existing liquid hydrocarbon distribution infrastructure emerge as additional advantageous features that strengthen the candidacy of methanol as an attractive alternative to liquid hydrocarbons.

Sufficiently detailed knowledge of the chemistry involved in the oxidation of methanol under most conditions of practical interest is available. A detailed mechanism was compiled by Westbrook and Dryer in 1980 [4] and a number of updated descriptions are currently accessible (see [5] for an extensive chronological list of mechanisms available prior to 2011). While detailed-chemistry descriptions extending beyond the C1 chemistry require consideration of a few hundred reactions among several dozen species, shorter mechanisms are useful for describing many features of methanol combustion. An example of these short-chemistry descriptions, obtained by eliminating reactions of lesser importance, is the 17-species and 40-step scheme proposed by Liao et al. [5].

Even simpler chemistry descriptions, involving fewer relevant chemical species and a reduced number of overall reactions, follow from introducing steady-state approximations for intermediaries whose rates of production and consumption are large compared with their transport rate. The associated reduced mechanisms result in shorter computational times, while providing sufficient accuracy to yield reliable computational results. For methanol, this strategy has been pursued in seeking reduced descriptions for specific combustion conditions, yielding different mechanisms for premixed combustion [6, 7], nonpremixed combustion [8, 9], and autoignition processes [10, 11]. In many combustion systems, however, it is not known in advance, at the start of a calculation, in exactly what manner the combustion will develop. That is often the case in spray-combustion systems, in which we may find regions in the combustor where autoignition and premixed-flame propagation are the predominant combustion modes, where in others the fuel burns in a diffusion-controlled flame [12]. What is needed for these systems, therefore, is sufficiently accurate reduced chemistry that encompasses all of these combustion processes. The purpose of the present investigation is to derive such a systematically reduced description for methanol-oxygen combustion. Multipurpose reduced descriptions of this type are available for hydrogen [13, 14], for example, but none are yet available for methanol. Since the focus will be on fuel oxidation, rather than on pollutant generation, the slow chemistry associated with the production of nitrogen oxides, included specifically in the 23-species and 19-step reduced mechanism developed by Lindstedt and Meyer [15], will not be considered here, thereby simplifying considerably the description.

The development will begin by identifying the minimum set of reactions and chemical species needed to describe methanol combustion, including key magnitudes such as equilibrium temperatures and compositions, laminar burning rates, critical conditions for extinction, and autoignition times. The resulting skeletal mechanism comprises 17 chemical species and 38 elementary reactions, only 13 of which are reversible. Subsequent introduction of steady-state approximations for six species, to reduce the total number of reactive species out of steady state to eleven, leads to a reduced mechanism with eight overall reactions when the atom conservation equations for C, O, and H are additionally taken into account. It is seen that the associated global rates, expressed in terms of those of the elementary reactions, can be evaluated explicitly without necessitating truncation of the algebraic expressions for the steady-state species. The skeletal and reduced mechanisms are tested through comparisons of numerical results with detailed-chemistry computations using the complete C1-C3 San Diego mechanism [16] (247 reactions

and 50 species) and also through comparisons with available experimental measurements.

2. Development of the skeletal mechanism

The chemistry description presented in the original detailed mechanism proposed by Westbrook and Dryer in 1980 [4] was improved in somewhat later years, leading to more accurate kinetic schemes (e.g., [15–18]). Some of the improvements stemmed from the inclusion of additional elementary steps not considered in the early mechanism. For instance, reactions describing the H attack on CH_2OH to form CH_3 and others involving CH_3, CH_2, CH, and CH_3O were found to be necessary to improve accuracy in comparisons with experiments [19, 20]. Other improvements followed from modifications to the rates of important rate-controlling elementary reactions, in particular those involving the initiation steps [21, 22] and the fuel attack by radicals. An example of the latter is the rate constants of reactions $CH_3OH + OH \rightarrow CH_2OH + H_2O$ and $CH_3OH + OH \rightarrow CH_3O + H_2O$, whose temperature dependences, assumed to be identical in initial studies [19, 23], exhibit differences that were accounted for to quantify better the CH_3O yield at high temperatures [20]. An additional modification to the rate of the reaction $CH_3OH + H \rightarrow CH_2OH + H_2$ was introduced subsequently [21] to be needed to describe better the effect of temperature on the total consumption rate of CH_3OH in counterflow diffusion flames.

In the following, we shall consider the complete San Diego mechanism [16] as a basis for comparison with the predictions of the skeletal and reduced mechanisms derived below. Correspondingly, the rate parameters of the most updated version of this mechanism [16] have been employed in evaluating the rates of the different elementary reactions of the skeletal and reduced mechanisms. It is worth mentioning that the computations reported below motivated a change in one of the reaction rates used in the San Diego mechanism, namely that of the hydroperoxyl-consumption reaction $HO_2 + OH \rightleftharpoons H_2O + O_2$, now assigned the two-term bi-Arrhenius expression recommended by Hong et al. [25], including a term with negative activation energy to describe the low-temperature range. The previous rate selection [24] was also a two-term expression with the positive-activation-energy term of [25], but employing instead the rate parameters suggested in [26] for the negative-activation-energy term. The methanol computations carried out in this study revealed that the premixed-flame propagation velocity is very sensitive to the rate of this elementary step and that use of the rate parameters of [25] for both terms in the bi-Arrhenius expression improves considerably the accuracy of the comparisons with experiments, especially at the higher pressures, thereby motivating the modification adopted, which also improves agreement with the experimental results reported in [27].

In using the current San Diego mechanism as the basis for comparison of the present reductions, it is important to identify the range of conditions over which that mechanism is designed to apply. It is developed for application to combustion problems under prevalent conditions of interest. Specifically, temperatures between roughly 1000 K and 3000 K, pressures including about 1 atm to 10 atm, and equivalence ratios of premixed systems between about 0.5 and 2.0 are addressed, although atmospheric diffusion flames, portions of which are outside this range of equivalence ratio, also are included, and additions have been recently made to encompass some lower-temperature aspects of NTC chemistry. Methanol portions of that mechanism, including methoxy and hydroxy methyl reactions, have not

been up-dated recently, and the only specifically methanol-related falloff is that for splitting off OH from CH_3 in methanol. These limitations are especially noteworthy in view of extensive research during the last five years on the chemical kinetics of methanol and related systems [28–36]. Further reference to research prior to 2014 may be found in a recent review [37]. While many of the new investigations concern conditions at higher pressures and lower temperatures than those identified above (conditions which, however, also are of considerable interest in combustion, even though very few applications of the new results to premixed or diffusion flames have been reported), the new results may well have significant implications for the rate parameters in the mechanism that was selected as the basis for the present work. Despite whatever deficiencies may exist in the basis mechanism, the good agreement of its predictions with the experiments to be addressed here (coupled with its relative simplicity), to be seen later, is considered to constitute sufficient motivation for its selection.

A first step towards reducing chemical-kinetic mechanisms is to identify a skeletal mechanism, in which a number of species and steps are eliminated to facilitate proceeding with a systematic reduction. While many compilations of skeletal mechanisms use the complete detailed description as a starting point and proceed by discarding elementary reactions with negligible influence, in the present development we choose an alternative strategy, taking an opposite approach, by extending the successful 27-step ignition mechanism of Seiser et al. [11] to achieve sufficiently accurate predictions of other combustion processes. It was found that, by addition of 11 elementary reactions, needed to ensure reasonable accuracy in computations of premixed and nonpremixed flames, a suitable skeletal mechanism could be obtained.

The selection of the additional reactions was guided by the previous work by Zhang et al. [38], Card et al. [39] and Yang et al [40], leading to the skeletal scheme shown in Table 1. The resulting description, restricted to C1 chemistry, involves 17 reactive species and 38 elementary reactions. The same species are considered in the short mechanism of Liao et al. [5], which contains, however, 40 reactions. Unlike the previous compilation, the fuel-attack step $CH_3OH + H \rightarrow CH_3O + H_2$ was not included in this skeletal mechanism, because it was found to be unimportant under the whole range conditions explored in the investigation, nor were the methoxy-radical consumption steps retained, since they, too, were found inconsequential, and they are not in the detailed San Diego mechanism [16], in which methoxy largely isomerizes to the more stable hydroxy methyl prior to its consumption. By way of contrast, the methanol dissociation reaction $CH_3OH + M \stackrel{38}{\rightarrow} CH_3 + OH + M$, not present in [5], is retained here because of its essential role in describing high-temperature autoignition events [11] with this mechanism. Another noticeable difference is that, while all 40 reactions in [5] are reversible, in the present mechanism the backward rates of only 13 reactions are considered in Table 1, the remaining 25 reverse steps having been found to exert a negligible influence in all cases studied.

3. Derivation of the systematically reduced eight-step mechanism

The reduction continues by introducing steady-state assumptions for intermediates, an approximation that is very accurate for HCO, CH_3O, CH_4, CH_3, O, and CH_2OH, as indicated by our computations. Our decision to test the steady states for these particular species was based on previous experience. The tests were made by calculating the relative fractional differences between the production and con-

sumption rates $|(\omega_p - \omega_c)/\max(\omega_p, \omega_c)|$ in the test problems to be discussed later and requiring the relative fractional differences to be sufficiently small, always less than 0.1, for example. Further tests were based on comparisons of predictions with experimental measurements, presented later. While the validity of the steady states fo the radicals is perhaps not surprising, the steady state for CH_4 may not have been expected. This occurs because, like the steady state for H_2O_2 in high temperature combustion processes, for example, in the methanol chemistry CH_4 is created in very small concentrations as a side reaction and is then efficiently consumed by radicals.

With these approximations, the chemistry of methanol oxidation reduces to the eight overall steps

$$
\begin{aligned}
3\,H_2 + O_2 &\overset{\text{I}}{\rightleftharpoons} 2\,H_2O + 2\,H \\
H_2 + OH &\overset{\text{II}}{\rightleftharpoons} H_2O + H \\
H + H + M &\overset{\text{III}}{\rightleftharpoons} H_2 + M \\
HO_2 + H &\overset{\text{IV}}{\rightleftharpoons} 2\,OH \\
H_2O_2 + M &\overset{\text{V}}{\rightleftharpoons} 2\,OH + M \\
CO + H_2O &\overset{\text{VI}}{\rightleftharpoons} CO_2 + H_2 \\
CH_2O &\overset{\text{VII}}{\rightleftharpoons} CO + 2H \\
CH_3OH + O_2 &\overset{\text{VIII}}{\rightleftharpoons} CH_2O + H_2O_2
\end{aligned}
$$

with rates (moles per unit volume per unit time) given in terms of the different elementary-reaction rates by the expressions

$$
\begin{aligned}
\omega_{\text{I}} &= \omega_1 + \omega_5 - \omega_8 - \omega_{10} - \omega_{11} - \omega_{13} + \omega_{18} \\
&\quad + \omega_{26} - \omega_{28} - \omega_{29} - \omega_{31} + \omega_{32} - \omega_{34} + \omega_{37} - \omega_{38}, && (1) \\
\omega_{\text{II}} &= -2\omega_1 + \omega_3 - \omega_4 + \omega_5 - 2\omega_5 + 2\omega_8 + \omega_9 + 2\omega_{10} + 3\omega_{11} \\
&\quad + 2\omega_{13} + \omega_{14} + \omega_{17} - 2\omega_{18} + \omega_{21} - 2\omega_{26} + 2\omega_{28} \\
&\quad + 2\omega_{29} + \omega_{33} + 2\omega_{31} - 2\omega_{32} + 3\omega_{34} - 2\omega_{37} + 2\omega_{38}, && (2) \\
\omega_{\text{III}} &= \omega_5 + \omega_6 - \omega_{13} + \omega_{16} + \omega_{17} + \omega_{18} + \omega_{19} + \omega_{20} + \omega_{21} + \omega_{25} \\
&\quad + \omega_{26} - \omega_{31} + \omega_{32} + \omega_{33} + \omega_{35} + \omega_{37}, && (3) \\
\omega_{\text{IV}} &= -\omega_5 + \omega_7 + \omega_8 + \omega_9 + \omega_{10} + \omega_{11} + 2\omega_{13} - \omega_{18} + \omega_{22} - \omega_{26} + \omega_{28} \\
&\quad + \omega_{29} + \omega_{31} - \omega_{32} - \omega_{33} - \omega_{35} - 2\omega_{37}, && (4) \\
\omega_{\text{V}} &= \omega_{12} - \omega_{13} - \omega_{22} + \omega_{33} + \omega_{34} + \omega_{35} + \omega_{37} + \omega_{38}, && (5) \\
\omega_{\text{VI}} &= \omega_{14}, && (6) \\
\omega_{\text{VII}} &= \omega_{19} + \omega_{20} + \omega_{21} + \omega_{22}, && (7) \\
\omega_{\text{VIII}} &= \omega_{33} + \omega_{34} + \omega_{35} + \omega_{36} + \omega_{37} + \omega_{38}. && (8)
\end{aligned}
$$

The concentrations of the steady-state species, needed for the evaluation of the above elementary rates, can be computed in terms of those of the eleven reactive species retained in the reduced description (CH_3OH, O_2, CO_2, H_2O, H_2, CO, H, OH, HO_2, H_2O_2, and CH_2O) through

$$C_{\rm O} = \frac{k_{1\,\rm f}C_{\rm H}C_{\rm O_2} + k_{2\,\rm b}C_{\rm OH}C_{\rm H} + k_{4\,\rm b}C_{\rm OH}C_{\rm OH} + k_{9\,\rm f}C_{\rm HO_2}C_{\rm H}}{k_{1\,\rm b}C_{\rm OH} + k_{2\,\rm f}C_{\rm H_2} + k_{4\,\rm f}C_{\rm H_2O} + k_{9\,\rm b}C_{\rm H_2O} + k_{10\,\rm f}C_{\rm HO_2} + k_{20\,\rm f}C_{\rm CH_2O}}, \tag{9}$$

$$C_{\rm CH_2OH} = C_{\rm CH_3OH} \times (A/B), \tag{10}$$

$$C_{\rm HCO} = C_{\rm CH_2O}\frac{k_{19\,\rm f}C_{\rm H} + k_{20\,\rm f}C_{\rm O} + k_{21\,\rm f}C_{\rm OH} + k_{22\,\rm f}C_{\rm HO_2}}{k_{15\,\rm f}C_{\rm M_4} + k_{16\,\rm f}C_{\rm H} + k_{17\,\rm f}C_{\rm OH} + k_{18\,\rm f}C_{\rm O_2}}, \tag{11}$$

$$C_{\rm CH_3O} = \frac{k_{32\,\rm b}C_{\rm CH_2OH}C_{\rm M_5} + k_{34\,\rm f}C_{\rm CH_3OH}C_{\rm OH}}{k_{26\,\rm f}C_{\rm O_2} + k_{27\,\rm f}C_{\rm M_5} + k_{32\,\rm f}C_{\rm M_5}}, \tag{12}$$

$$C_{\rm CH_4} = \left(\frac{k_{29\,\rm f}C_{\rm CH_2OH}C_{\rm H} + k_{38\,\rm f}C_{\rm CH_3OH}}{k_{23\,\rm f}C_{\rm H}}\right)\left(\frac{k_{23\,\rm b}C_{\rm H_2} + k_{25\,\rm f}C_{\rm H}}{k_{24\,\rm f}C_{\rm O} + k_{29\,\rm b}C_{\rm OH}}\right), \tag{13}$$

$$C_{\rm CH_3} = \frac{k_{29\,\rm f}C_{\rm CH_2OH}C_{\rm H} + k_{38\,\rm f}C_{\rm CH_3OH}}{k_{24\,\rm f}C_{\rm O} + k_{29\,\rm b}C_{\rm OH}}, \tag{14}$$

obtained by algebraic manipulation of the steady-state equations, with the compact expressions

$$A = \frac{k_{32\,\rm f}k_{34\,\rm f}C_{\rm OH}}{k_{26\,\rm f}C_{\rm O_2}/C_{\rm M_5} + k_{27\,\rm f} + k_{32\,\rm f}} + k_{33\,\rm f}C_{\rm OH} + k_{35\,\rm f}C_{\rm H} + k_{36\,\rm f}C_{\rm HO_2} + k_{37\,\rm f}C_{O2} \tag{15}$$

$$B = C_{\rm H}(k_{28\,\rm f} + k_{29\,\rm f}) + k_{30\,\rm f}C_{\rm O_2} + C_{\rm M_5}(k_{31\,\rm f} + k_{32\,\rm b}) - \frac{k_{29\,\rm f}C_{\rm H}}{(k_{24\,\rm f}/k_{29\,\rm b})(C_{\rm O}/C_{\rm OH}) + 1} - \frac{k_{32\,\rm b}C_{\rm M_5}}{(k_{26\,\rm f}/k_{32\,\rm f})(C_{\rm O_2}/C_{\rm M_5}) + k_{27\,\rm f}/k_{32\,\rm f} + 1}$$

introduced in (10) for writing the concentration of hydroxymethyl. The subscripts f and b are used in (9)–(15) to denote the forward and backward rate constants for the reactions in Table 1. The order in which the expressions (9)–(14) are arranged is intended to facilitate the evaluation, in that the concentration of O is to be computed first, followed by that of CH_2OH, which depends on $C_{\rm O}$, and those of the remaining steady-state species, which exhibit dependences on $C_{\rm O}$ and/or $C_{\rm CH_2OH}$.

It is of interest that, besides the six steady-state species in (9)–(14), OH also was found to follow a good steady-state approximation in all of the test cases. An accurate seven-step reduced mechanism therefore exists. An explicit description such as that given above, however, could not be derived when OH was placed in steady state because OH is so strongly coupled to the other species. Although automatic programs capable of handling complex systems of algebraic equations would enable the use of a seven-step mechanism, readily derived from the eight-step mechanism by use of step II in steps IV and V, the small advantage in going from eight to seven steps, with ten rather than eleven reactive species, seems more than offset by the relative simplicity of the explicit result.

4. Test for equilibrium conditions

A first set of computations pertains to adiabatic equilibrium states, with results shown in Fig. 1 for a methanol-air mixture of varying equivalence ratio ϕ at normal atmospheric initial conditions. As can be seen, the adiabatic flame temperature and the associated equilibrium mass fractions of CO_2, H_2O, CO, and H_2 obtained with the skeletal and reduced mechanisms, indicated by the solid and dashed curves, respectively, are indistinguishable from the values obtained with the detailed chemistry, denoted by symbols, except for very rich mixtures, where small relative deviations of the results of the skeletal mechanism are observed, although the extent of the departures is quite limited. The plots seem to indicate that the minor species that are left out of the skeletal mechanism, and that therefore do not appear in Fig. 1, are in fact present in larger concentrations for richer mixtures, which would explain the increasing deviations seen in the figure. In addition, it was found that the steady-state approximations introduced in developing the reduced chemistry (especially that for CH_4) modify the species balance in such a way that the agreement with the detailed-chemistry results is unexpectedly improved in Fig. 1. There is similar agreement at other initial conditions, such as elevated pressures or initial temperatures. It is worth emphasizing that not all potential reductions preserve this degree of agreement; there were notable differences in some of our earlier attempts.

FIGURE 1 HERE

5. Test for burning velocities of laminar premixed flames

To test the degree of accuracy of the chemistry simplifications, results of computations employing the skeletal and reduced mechanisms were compared with detailed-chemistry computations and also with experimental measurements. These computations include premixed and nonpremixed flames with different transport descriptions and homogeneous-ignition histories. The flame computations were carried out using an in-house finite-difference code, validated earlier through extensive comparisons with widely employed commercial codes [42, 43]. Besides a detailed multicomponent species-transport description including thermal diffusion (see [44] for details of the associated transport equations), two simpler transport descriptions are available in our code, namely, a mixture-average model, details of which can be found in the CHEMKIN transport documentation [42], and the constant-Lewis-number approximation proposed by Smooke and Giovangigli [45]. When using the latter, the value $L_{CH_3OH} = 1.3$ was adopted for the Lewis number of methanol, while for the other species the values employed are those listed in [45].

The curves in Fig. 2 represent the variation of the flame velocity with the equivalence ratio for $p = 1$ atm and $p = 10$ atm obtained from numerical integrations with detailed, short, and reduced chemistry descriptions. In premixed-flame computations, the results were found to be largely independent of the species-transport description employed, in that the velocities calculated with the mixture-average model, shown in Fig. 2, differ by less than 2 % from those computed with the more involved multicomponent model and also with those using the constant-Lewis-number approximation. Furthermore, in the tests employing the multicomponent transport model, negligible differences in resulting flame speeds were observed when the thermal-diffusion terms were selectively removed from the diffusive fluxes of the

different chemical species, indicating that Soret effects are unimportant in methanol premixed combustion. These observations document the utility of such simplified transport descriptions for steady, planar premixed flames, even though they could introduce inaccuracies in unsteady or nonplanar cases.

FIGURE 2 HERE

The numerical results are compared with the most recent experimental measurements reported in the literature [46–49]. Earlier experiments [19, 50–53] show significant scatter and have not been included in the figure to avoid unnecessary clutter. The comparisons with the experimental data indicate that the three chemistry descriptions give satisfactory results both at atmospheric and elevated pressures. Although the skeletal and reduced mechanisms predict velocities that differ from those of the detailed chemistry (i.e., overpredictions of the order of 10% for lean and stoichiometric mixtures and somewhat smaller underpredictions for rich mixtures with equivalence ratios $\phi \gtrsim 1.3$), the associated deviations are acceptable for practical purposes, in that they are comparable in magnitude to the experimental uncertainty present in measurements of flame propagation velocities. The agreement between the results of the reduced mechanism and those of the 38-step skeletal chemistry, with observed differences amounting to just a few percent over the whole range of compositions tested, is a indication of the accuracy of the steady-state approximations introduced in developing the reduced chemistry.

The predictive capabilities of the skeletal and reduced mechanisms are tested further in Fig. 3 in connection with the dependence of the propagation velocity of a stoichiometric methanol-air flame on the initial temperature and pressure. The figure includes experimental measurements collected from a number of recent studies for stoichiometric methanol-air mixtures [46, 47, 54–56], along with numerical computations with detailed, skeletal, and reduced chemistry. As can be seen, the detailed-chemistry results are in close agreement with the experimental measurements, although they tend to overpredict experimental data at elevated temperatures (even though by a lesser amount than the difference between different experiments). On the other hand, the skeletal and reduced mechanisms tend to overpredict the flame propagation by amounts up to 20%, but still comparable with the departures observed in different experiments. Despite these differences, both simplified descriptions, in close agreement with each other, adequately predict the pronounced decrease (increase) of flame velocity with increasing pressure (temperature) observed in experiments. Since it was found that agreements of flame-speed predictions of the skeletal mechanism with those of the detailed mechanism could be improved appreciably only by enlarging the skeletal mechanism substantially, it was felt that this 38-step mechanism afforded the best compromise.

FIGURE 3 HERE

6. Ignition tests

Results of experiments on the ignition of methanol vapor, carried in a nitrogen stream, counterflowing against a heated oxidizer stream have been addressed previously [11]. In that work, the temperature of the oxidizer stream required for autoignition to occur, measured as a function of the strain rate of the counter-

flow, was found to be in excellent agreement with computations based on both detailed chemistry and a six-step systematically reduced mechanism. Since the present eight-step mechanism is an augmentation of that six-step mechanism, extending it to encompass flames, the same agreement will be obtained. For that reason, such comparisons are not shown here. Attention instead is directed towards ignition times of homogeneous mixtures measured in shock-tube experiments under conditions for which our reduced mechanism is designed to apply.

Autoignition times of methanol-air mixtures (upper plot) and methanol-oxygen-argon mixtures (lower plot), obtained with the different chemistry descriptions from homogeneous adiabatic ignition computations in an isochoric reactor, are compared in Fig. 4 with shock-tube experimental measurements [57–60]. Although the selection of the criterion used to define the ignition time in computations is not critical, in that quantitative differences between results based on different criteria were found to be always very small for these methanol cases, in the computations the criterion employed was adapted to match as closely as possible that used in the different experiments whenever that could be done. For instance, in the computations for the experiments with p between 1.2 and 1.75 atm, ignition was identified by the maximum of the product of the concentrations of O and CO, in agreement with the criterion used in the corresponding experiments [58], while for $p = 0.33$ atm the ignition was taken to occur when the maximum growth rate of C_{CO2} is achieved, that being the experimental criterion used in [57]. The criteria used to determine the ignition time in the other experiments of Fig. 4 (i.e., the emission of visible light in the experiments of Natarajan et al. [59] at $p = 2.5$ atm and $p = 4.5$ atm and the appearance of shock waves arising from secondary explosions in the methanol-air experiments of Fieweger et al. [60]) could not be evaluated in our computations. For those experiments, the numerical results shown in Fig. 4 employed as the ignition criterion the maximum of the CO_2 production rate, which gives results that are almost identical to those of the common temperature-inflection criterion, not used in any of the evaluations of Fig. 4.

FIGURE 4 HERE

It is seen in Fig. 4 that reasonably good agreement is obtained between the computational results using different chemistry models, and also between the computational results and most of the experiments. Larger discrepancies are observed at higher temperatures, especially in connection with the reduced-chemistry model, which gives overpredictions in ignition times that reach 40 % as the temperature approaches $T = 2000$ K. These latter overpredictions are mainly attributable to the steady-state assumptions of CH_3 and CH_4, which become less accurate during ignition events at higher temperatures. The agreement improves considerably at lower temperatures, with the different curves becoming indistinguishable below a given limiting temperature, which is higher for higher pressures (e.g., for $T \lesssim 1300$ K at $p = 1$ atm). Despite the departures in ignition-time predictions, more prominent at low pressure and high temperature (where disagreements are noticeable even for the detailed mechanism), the degree of accuracy of the reduced mechanism displayed in Fig. 4 is clearly satisfactory for the conditions found in most combustion applications, as could be expected from the previous investigations [11]. For these reasons it may be concluded that the skeletal and reduced mechanisms are both adequate for the major ignition problems of interest.

7. Tests for structures of counterflow flames

A great deal of detail can be found in measurements of structures of counterflow flames [21, 61, 62]. The data available, including temperature profiles measured with fine thermocouples and concentration profiles of stable chemical species measured by gas sampling followed by gas chromatography, were obtained in these experiments for diffusion flames as well as for partially premixed flames, with fuel-side equivalence ratios down to 2.0 [21, 61], but under diluted conditions, the fuel vapor being carried by a nitrogen stream, to improve the accuracies of the measurements, over those available in earlier measurements of counterflow flames above vaporizing liquid-fuel pools, as referenced previously [62]. The most recently reported diffusion-flame measurements [62] are selected here for comparisons, although similar agreements would be expected for the partially premixed flames [21, 61]. While radical profiles, not available experimentally, would provide sharper tests, the profiles of the stable species afford some basis for evaluation. Figure 5 compares measurements and predictions for both the skeletal and reduced mechanisms.

FIGURE 5 HERE

For the conditions examined, corresponding to a strain rate $A = 100$ s^{-1} that places the flame far from extinction, the skeletal mechanism is seen to reproduce accurately the profiles of temperature and main species, including those of the intermediates H_2 and CO. The slight broadening of the experimental temperature profiles in the wings is attributable to the thermocouple resolution [63]. The reduced mechanism also produces satisfactory results, except for H_2, whose production rate is underpredicted, leading to a peak value that is about 20% too low. To overcome the drawback that the experiments did not provide measurements of radicals, for completeness the figure includes in an inset the profiles of O, OH, and H obtained numerically, showing no significant differences between the results of the skeletal and reduced mechanisms. In particular, the remarkable agreement between the profile of CO determined from the skeletal mechanism and that evaluated from (9) in the computations with reduced chemistry is an indication of the excellent accuracy of the steady-state approximation for this species.

The figure also includes as dashed curves results of computations performed with a simple constant-Lewis-number model for species transport in the 38-step chemistry. The resulting curves lie close to the thick solid curves, obtained with multicomponent transport with the same chemistry description. This may be attributed to the fact that, for the specific dilute conditions examined in the plot, nitrogen is the most abundant species all across the mixing layer. Under that condition the approximation of constant Lewis numbers becomes quite accurate. On the other hand, larger departures would be expected if undiluted fuel feed were considered. In general, then, these favorable comparisons of profiles further support the utility of the skeletal and reduced mechanisms.

8. Tests for critical conditions for extinction of counterflow flames

Predictions of critical conditions for extinction of counterflow flames typically provide the most stringent tests of chemical-kinetic and transport approximations in that extinction predictions generally are strongly sensitive to those parameters. In the present work, the experimental results of Seiser et al. [62] were used to test the

accuracy of the simplified chemistries under nonpremixed combustion conditions. In the experiments that exhibited the best agreement with predictions, the critical strain rate at extinction A_E of counterflow diffusion flames was measured in an opposed-jet facility involving a stream of methanol diluted with nitrogen counterflowing against an air stream with stream temperatures fixed but methanol concentrations varied. For a given value of the methanol mass fraction in its feed stream, $Y_{\mathrm{CH_3OH}}$, the counterflow strain rate $A = 2\left[1 + V_{fuel}\sqrt{\rho_{fuel}}/(V_{air}\sqrt{\rho_{air}})\right]\,(V_{air}/L)$, defined in terms of the distance L between the nozzle exists and the densities and velocities of the fuel and air streams, was increased by increasing the flow velocities, maintaining a momentum balance to fix the flame position, until extinction was achieved. The procedure was repeated for several values of the fuel mass fractions, giving the results represented with symbols in Fig. 6, which are compared with results of numerical computations obtained with the detailed, skeletal, and reduced mechanisms.

FIGURE 6 HERE

The numerical results compare favorably with experiments, with all three mechanisms yielding values of A_E that differ from the experimental measurements by relatively small amounts, comparable to the experimental scatter observed in the plot. Specifically, compared with the detailed-chemistry results, represented by a solid curve, the skeletal mechanism is seen to give small overpredictions of A_E on the order of 5 % for all dilutions considered in the figure. On the other hand, because of the steady-state approximations present in the reduced chemistry, the predicted values of A_E are smaller than those of the skeletal mechanism by an amount that exceeds 5 %, so that the corresponding chain curve in Fig. 6 lies below the detailed-chemistry curve.

Although all of the computations shown in Fig. 6 were performed with a mixture-average transport model, additional computations with the multicomponent and constant-Lewis-number models were used to test the influence of the transport description on the resulting predictions. As could be expected from previous comparative studies [64], for nonpremixed conditions the transport model used was found to have a nonnegligible influence on the solution, although the differences between the multicomponent and mixture-average models were small, leading to predictions of A_E that are about 3 % lower for the former. The departures observed when the constant-Lewis-number description is employed are significantly larger. Irrespective of the chemistry, the use of the constant-Lewis-number approximation consistently gives values of A_E smaller than those of the other transport models, with differences with the mixture-average results shown in the figure being on the order of 15 % over the whole range of fuel-stream dilutions considered. It is also of interest that no significant quantitative differences were observed when removing the thermal-diffusion terms in the multicomponent-transport computations, indicating that, just like in the flame-speed tests, Soret transport has a negligible influence also on the critical extinction conditions of methanol diffusion flames.

Data also were obtained [62] on the extinction of premixed counterflow flames of mixtures of methanol, oxygen, and nitrogen flowing against oxygen-nitrogen mixtures. Strain rates at extinction were measured for stoichiometric mixtures as a function of the oxygen concentration in the oxidizer stream and also as a function of the fuel-stream equivalence ratio for a fixed composition of the oxidizer stream. In these cases, the disagreement between the computational and experimental results was found in that paper to be much larger than that in Fig. 6. By and large, that

disagreement persists even in the current version of the San Diego mechanism. That is, despite the improvements in the detailed chemistry, comparable disagreements remain, pointing to the need for further investigations, making use of the more recent chemical-kinetic studies cited earlier. The influences associated with the skeletal and reduced chemistry, as well as with the different transport descriptions, however, remain comparable to those illustrated in Fig. 6 for this test.

9. Concluding remarks

It is clear from this work that, despite the successes of the San Diego mechanism, further study of the individual steps and associated rate parameters in that mechanism is warranted. Nevertheless, it seems likely that, whatever future revisions arise in the mechanism, either the present skeletal 38-step mechanism or a mechanism very much like it will be able, with correspondingly revised elementary rate parameters, to provide good predictions for combustion processes of interest, exhibiting, for example, differences from burning-velocity predictions of the detailed mechanism on the order of about 10 % at most. Perhaps more importantly, by introducing chemical-kinetic steady-state approximations for the relevant intermediate species, a reduced-chemistry description has been derived, which leads to predictions in close agreement with those of the skeletal mechanism in all cases tested. That mechanism, which involves only 8 overall steps among 11 reactive chemical species, was obtained by beginning with a similar 6-step mechanism applicable only to autoignition processes and then extending it, on the basis of the 38-step mechanism, to include the flames that arise in other combustion processes. That extension is associated mainly with the chemistry of HO_2 and H_2O_2, augmenting that chemistry to include H and OH as species that are not placed in a steady state, the former departing substantially from steady-state behavior in combustion processes other than ignition.

This new 8-step mechanism can facilitate computational investigations of systems for which both autoignition and premixed or diffusion flames may occur, when the detailed or skeletal chemistry is too extensive to be employed economically. An explicit computational approach, namely first equation (9), then (15), followed by (10)–(14), is given for implementing the reduction efficiently. Computational approaches to broad-range combustion problems that previously were available only for simpler fuels, such as hydrogen, are now extended in this work to methanol. Besides the gains associated with the simplified evaluation procedure for the chemical rates and the consideration of a reduced number of conservation equations for the chemical species, the robustness of the reduced chemistry enables larger time steps to be implemented in numerical integrations without compromising the accuracy of the results, thereby reducing computational costs significantly, as quantified in the appendix.

In the validation investigations performed here in connection with these developments, previous ideas concerning influences of different descriptions of transport properties were confirmed, and it was found that, contrary to combustion processes of hydrogen, Soret diffusion is inconsequential for methanol. In addition, the computations indicate that for methanol combustion the mixture-average transport model gives sufficient accuracy for all conditions tested in the paper. Its use in combination with the reduced chemistry can help reduce computational times significantly.

Acknowledgements

This work was supported by the Spanish MCINN through projects # CSD2010-00011, ENE2012-33213 and ENE2015-65852-C2-1-R.

References

[1] J. Vancoillie, J. Demuynck, L. Sileghem, M. Van De Ginste, S. Verhelst, L. Brabant, L. Van Hoorebeke, *The potential of methanol as a fuel for flex-fuel and dedicated spark-ignition engines*, Applied Energy 102 (2013), pp. 140–149.

[2] T. Fleisch, C. McCarthy, A. Basu, C. Udovich, P. Charbonneau, W. Slodowske, S.-E. Mikkelsen, J. McCandless, *A New Clean Diesel Technology: Demonstration of ULEV Emissions on a Navistar Diesel Engine Fueled with Dimethyl Ether*, SAE Technical Paper 950061, 1995, doi:10.4271/950061.

[3] M.J. Brusstar, C.L. Gray Jr., Society of Automotive Engineers, *High Efficiency with Future Alcohol Fuels in a Stoichiometric Medium Duty Spark Ignition Engine*, SAE paper 2007-01-3993 (2007).

[4] C.K. Westbrook, F.L. Dryer, *A Comprehensive Mechanism for Methanol Oxidation*, Combust. Sci. Technol. 20 (1979), pp. 125–140.

[5] S.Y. Liao, H.M. Li, L. Mi, X.H. Shi, G. Wang, Q. Cheng, C. Yuan, *Development and Validation of a Reduced Chemical Kinetic Model for Methanol Oxidation*, Energy Fuels 25 (2011), pp. 60–71.

[6] C.M. Mueller, N. Peters, *Reduced Kinetic Mechanisms for Premixed Methanol Flames*, in: N. Peters, B. Rogg (Eds.), Reduced Kinetic Mechanisms for Applications in Combustion Systems, Springer-Verlag, New York, 1993,, pp. 142–155.

[7] G. Paczko, P.M. Lefdal, N. Peters, *Reduced Reaction Schemes for Methane, Methanol and Propane Flames*, Proc. Combust. Inst. 21 (1986), pp. 739–748.

[8] J.-Y. Chen, *Reduced Reaction Mechanisms for Methanol-Air Diffusion Flames*, Combust. Science Tech. 78 (1991), pp. 127–145.

[9] C.M. Mueller, K. Seshadri, J.Y. Chen, *Reduced Kinetic Mechanisms for Counterflow Methanol Diffusion Flames*, in: N. Peters, B. Rogg (Eds.), Reduced Kinetic Mechanisms for Applications in Combustion Systems, Springer-Verlag, New York, 1993,, pp. 284–307.

[10] S. Yalamanchili, W.A. Sirignano, R. Seiser, K.Seshadri, *Reduced methanol kinetic mechanisms for combustion applications*, Combust. Flame 142 (2005), pp. 258–265

[11] R. Seiser, K. Seshadri, F.A. Williams, *Detailed and reduced chemistry for methanol ignition*, Combust. Flame 158 (2011), pp. 1667–1672.

[12] A.L. Sánchez, J. Urzay, A. Liñán, *The role of separation of scales in the description of spray combustion*, Proc. Combust. Inst. 35 (2015), pp. 1549–1577.

[13] P. Boivin, C. Jiménez, A.L. Sánchez, F.A. Williams, *An explicit reduced mechanism for H_2 – air combustion*, Proc. Combust. Inst. 33 (2011), pp. 517–523.

[14] P. Boivin, A.L. Sánchez, F.A. Williams, *Four-step and three-step systematically reduced chemistry for wide-range H_2–air combustion problems*, Combust. Flame 160 (2013), pp. 76–82.

[15] R.P. Lindstedt, M. P. Meyer, *A Dimensionally Reduced Reaction Mechanism for Methanol Oxidation*, Proc. Combust. Inst. 29 (2002), pp. 1395–1402.

[16] "Chemical-Kinetic Mechanisms for Combustion Applications", San Diego Mechanism web page, Mechanical and Aerospace Engineering (Combustion Research), University of California at San Diego (http://web.eng.ucsd.edu/mae/groups/combustion/mechanism.html), Version 2014-10-04.

[17] T.J. Held, F.L. Dryer, *A Comprehensive Mechanism for Methanol Oxidation*, Int. J. Chem. Kinet. 30 (1998), pp. 805–830.

[18] J. Li, Z. Zhao, A. Kazakov, M. Chaos, F.L. Dryer, J.J. Scire, *A Comprehensive Kinetic Mechanism for CO, CH_2O, and CH_3OH Combustion*, Int. J. Chem. Kinet. 39 (2007), pp. 109–136.

[19] F.N. Egolfopoulos, D.X. Du, C.K. Law, *A Comprehensive Study of Methanol Kinetics in Freely- Propagating and Burner-Stabilized Flames, Flow and Static Reactors, and Shock Tubes*, Combust. Sci. Technol. 83 (1992), pp. 33–75.

[20] GRI-mech Version 3.0, released 7/30/99, CHEMKIN-II format (htts://www.me.berkeley.edu/gri_mech/).

[21] S.C. Li, F. A. Williams, *Experimental and numerical studies of two-stage methanol flames*, Proc. Combust. Inst. 26 (1996), pp. 1017–1024.

[22] B.L. Zhang, F.A. Williams, *Alcohol Droplet Combustion*, Acta Astronautica 39 (1996), pp. 599–603.

[23] H.S.T. Driver, R.J. Hutcheon, R.D. Lockett, G.N. Robertson, H.-H. Grotheer, S. and Klem, Ber. Bunsenges, *Elementary Reactions in the Methanol Oxidation System. Part II: Measurement and Modeling of Autoignition in a Methanol-Fuelled Otto Engine*, Phys. Chem. 96 (1992), pp. 1376–1387.

[24] A.L. Sánchez, F.A. Williams, *Recent advances in understanding of flammability characteristics of hydrogen*, Prog. Energy Combust. Sci. 41 (2014), pp. 1–55.

[25] Z. Hong, K. Lam, R. Sur, S. Wang, D. Davidson, R. Hanson, *On the rate constants of OH + HO_2 and HO_2 + HO_2 : A comprehensive study of H_2O_2 thermal decomposition using multi-species laser absorption*, Proc. Combust. Inst. 34 (2013), pp. 565–571.

[26] D.L. Baulch, C.J. Cobos, R.A. Cox, C. Esser, P. Frank, Th. Just, J.A. Kerr, M.J. Pilling, J. Troe, R.W. Walker, J. Warnatz, *Evaluated Kinetic Data for Combustion Modelling*, J. Phys. Chem. Ref. Data 21 (1992), pp. 411–734.

[27] H. Hashemi, J. M. Christensen, S. Gersen, P. Glarborg, *Hydrogen oxidation at high pressure and intermediate temperatures: Experiments and kinetic modeling*, Proc. Combust. Inst. 35 (2015), pp. 553–560.

[28] I. M. Alecu, D. G. Truhlar, *Computational Study of the Reactions of Methanol with the Hydroperoxyl and Methyl Radicals. 1. Accurate Thermochemistry and Barrier Heights*, J. Phys. Chem. A 115 (2011), pp. 2811–2829.

[29] I. M. Alecu, D. G. Truhlar, *Computational Study of the Reactions of Methanol with the Hydroperoxyl and Methyl Radicals. 2. Accurate Thermal Rate Constants*, J. Phys. Chem. A 115 (2011), pp. 14599–14611.

[30] K. Kumar, C.-J. Sung, *Autoignition of Methanol: Experiments and Computations*, Int. J. Chem. Kinet. 43 (2011), pp. 175–184.

[31] R. Meana-Pañeda, D. G. Truhlar, A. Fernández-Ramos, *High-level direct-dynamics variational transition state theory calculations including multidimensional tunneling of the thermal rate constants, branching ratios, and kinetic isotope effects of the hydrogen abstraction reactions from methanol by atomic hydrogen*, J. Chem. Phys. 134 (2011) 094302.

[32] V. Aranda, J. M. Christensen, M. U. Alzueta, P. Glarborg, S. Gersen, Y. Gao, P. Marshall, *Experimental and Kinetic Modeling Study of Methanol Ignition and Oxidation at High Pressure*, Int. J. Chem. Kinet. 45 (2013), pp. 283–294.

[33] E. E. Dames, D. M. Golden, *Master Equation Modeling of the Unimolecular Decompositions of Hydroxymethyl (CH_2OH) and Methoxy (CH_3O) Radicals to Formaldehyde (CH_2O) + H*, J. Phys. Chem. A 117 (2013), pp. 7686–7696.

[34] W. K. Metcalfe, S. M. Burke, S. S. Ahmed, H. J. Curran, *A Hierarchical and Comparative Kinetic Modeling Study of C1 – C2 Hydrocarbon and Oxygenated Fuels*, Int. J. Chem. Kinet. 45 (2013), pp. 638–675.

[35] W. Ren, E. Dames, D. Hyland, D. F. Davidson, R. K. Hanson, *Shock tube study of methanol, methyl formate pyrolysis: CH_3OH and CO time-history measurements*, Combust. Flame 160 (2013), pp. 2669–2679.

[36] L. T. Zaczek, K. Y. Lam, D. F. Davidson, R. K. Hanson, *A shock tube study of CH_3OH + OH → Products using OH laser absorption*, Proc. Combust. Inst. 35 (2015), pp. 377–384.

[37] S. M. Sarathy, P. Oßwald, N. Hansen, K. Kohse-Höinghaus, *Alcohol combustion chemistry*, Prog. Energy Combust. Sci. 44 (2014), pp. 40–102.

[38] B.L. Zhang, J.M. Card, F.A. Williams, *Application of Rate-Ratio Asymptotics to the Prediction of Extinction for Methanol Droplet Combustion*, Combust. Flame 105 (1996), pp. 267–290.

[39] J. Card, R. Ryden, F. A. Williams, *Influences of Flame-Vortex Interactions on Formation of Oxides of Nitrogen in Curved Methane-Air Diffusion Flamelets*, Combust. Flame 105 (1996), pp. 373–380.

[40] B. Yang, K. Seshadri, N. Peters, *The asymptotic structure of premixed methanol-air flames*, Combust. Flame 91 (1992), pp. 382-398.

[41] R. G. Gilbert, K. Luther, J. Troe, *Theory of thermal unimolecular reactions in the fall-off range. II. Weak collision rate constant*, Ber. Bunsenges Phys. Chem. 87 (1983), pp. 169–177.

[42] R. J. Kee, F. M. Rupley, J. A. Miller, M. E. Coltrin, J. F. Grcar, E. Meeks, H. K. Moffat, A. E. Lutz, G. Dixon-Lewis, M. D. Smooke, J. Warnatz, G. H. Evans, R. S. Larson, R. E. Mitchell, L. R. Petzold, W. C. Reynolds, M. Caracotsios, W. E. Stewart, P. Glarborg, C. Wang, and Ola Adigun, *CHEMKIN Collection, Release 3.6*, Reaction Design, Inc., San

Diego, CA (2000)

[43] Cosilab Collection, Rotexo-Softpredict-Cosilab GmbH & Co. KG, Bad Zwischenahn (Germany), www.SoftPredict.com (2007).

[44] G. Dixon-Lewis, *Flame structure and flame reaction kinetics. II. Transport phenomena in multicomponent systems*, Proc. Royal Soc. London. Series A, 307 (1968) 111–135.

[45] M.D. Smooke, V. Giovangigli, *Formulation of the Premixed and Nonpremixed Test Problems*, in: M. D. Smooke (ed) *Reduced Kinetic Mechanisms and Asymptotic Approximations for Methane-Air Flames*, Springer-Verlag, 1991,, pp. 1–28.

[46] K. Saeed, C.R. Stone, *Measurements of the laminar burning velocity for mixtures of methanol and air from a constant-volume vessel using a multizone model*, Combust. Flame 139 (2004), pp. 152–166.

[47] J. Vancoillie, M. Christensen, E. J. K. Nilsson, S. Verhelst, A. A. Konnov, *Temperature Dependence of the Laminar Burning Velocity of Methanol Flames*, Energy and Fuels 26 (2012), pp. 1557–1564.

[48] L. Sileghem, V. A. Alekseev, J. Vancoillie, E. J. K. Nilsson, S. Verhelst, A. A. Konnov, *Laminar burning velocities of primary reference fuels and simple alcohols*, Fuel 115 (2014), pp. 32–40.

[49] J. Beeckmann, L. Cai, H. Pitsch, *Experimental investigation of the laminar burning velocities of methanol, ethanol, n-propanol, and n-butanol at high pressure*, Fuel 117 (2014), pp. 340–350.

[50] W. Wiser, G. R. Hill, *A Kinetic Comparison of the Combustion of Methyl Alcohol and Methane*, Proc. Combust. Inst. 5 (1955), pp. 553–558.

[51] G.J. Gibbs, H.F. Calcote, *Effect of Molecular Structure on Burning Velocity*, J. Chem. Eng. Data 4 (1959), pp. 226–237.

[52] O.L. Gulder, *Laminar Burning Velocities of Methanol, Ethanol and Isooctane-Air Mixtures*, Proc. Combust. Inst. 19 (1982), pp. 275–281.

[53] M. Metghachi, J.C. Keck, *Burning Velocities of Mixtures of Air with Methanol, Isooctane, and Indolene at High Pressure and Temperature*, Combust. Flame 48 (1982), pp. 191–210.

[54] S.Y. Liao, D.M. Jiang, Z.H. Huang, W.D. Shen, C. Yuan, Q. Cheng, *Laminar burning velocities for mixtures of methanol and air at elevated temperatures*, Energy Convers. Mngt. 48 (2007), pp. 857–863.

[55] Z. Zhang, Z. Huang, X. Wang, J. Xiang, X. Wang, H. Miao, *Measurements of laminar burning velocities and Markstein lengths for methanol–air–nitrogen mixtures at elevated pressures and temperatures*, Combust. Flame 155 (2008), pp. 358–368.

[56] P.S. Veloo, Y.L. Wang, F.N. Egolfopoulos, C.K. Westbrook, *A comparative experimental and computational study of methanol, ethanol, and n-butanol flames*, Combust. Flame 157 (2010), pp. 1989–2004.

[57] D. Cooke, M. Dodson, A. Williams, *A Shock-Tube Study of the Ignition of Methanol and Ethanol with Oxygen*, Combust. Flame 16 (1971), pp. 233–236.

[58] C.T. Bowman, *A Shock-Tube Investigation of the High-Temperature Oxidation of Methanol*, Combust. Flame 25 (1975), pp. 343–354.

[59] K. Natajaran, K.A. Bhaskaran, *An Experimental and Analytical Study of Methanol Ignition Behind Shock Waves*, Combust. Flame 43 (1981), pp. 35–49.

[60] K. Fieweger, R. Blumenthal, G. Adomeit, *Self-Ignition of S.I. Engine Model Fuels: A Shock Tube Investigation at High Pressure*, Combust. Flame 109 (1997), pp. 599–619.

[61] S. C. Li, F. A. Williams, *Formation of NO_x, CH_4, and C_2 species in laminar methanol flames*, Proc. Combust. Inst. 27 (1998), pp. 485–493.

[62] R. Seiser, S. Humer, K. Seshadri, E. Pucher, *Experimental investigation of methanol and ethanol flames in nonuniform flows* Proc. Combust. Inst. 31 (2007), pp. 1173–1180.

[63] U. Niemann, K. Seshadri, F. A. Williams, *Effect of pressure on structure and extinction of near-limit hydrogen counterflow diffusion flames*, Proc. Combust. Inst. 34 (2013), pp. 881–886.

[64] B. A. Williams, *Sensitivity of Calculated Extinction Strain Rate to Molecular Transport Formulation in Nonpremixed Counterflow Flames*, Combust Flame 124 (2001), pp. 330–333.

Appendix A. Computational Savings

Measures of the significant gains in execution times that can be obtained by using the 8-step mechanism instead of the 38-step mechanism arise from different sources. The gain coming from the pure-chemistry (autoignition problem) evaluation was found to be only about 20%, compared with the skeletal mechanism. More significantly, the reduced chemistry was found to reduce the stiffness of the problem, allowing a larger time step to be used, issue especially relevant for explicit computational schemes. This is not a general result of reduced chemistry but was seen computationally to occur for the reduction developed here. The extent of the time-step increase depends on the specific conditions of the simulation; taken as a reference the time step needed for the 38-step skeletal mechanism, the factor by which this time step can be multiplied was roughly estimated to be in the range of a factor of 3 or 4 for lean flames, decreasing to a factor 2 for rich flames.

An additional advantageous feature of the reduced mechanism is the limited number of conservation equations for reactive species that need to be integrated; i.e., only 11, to be compared with the 17 and 50 equations corresponding to the skeletal and detailed mechanisms, respectively. The relative gain in computational time associated with the decrease in the number of chemical species depends on the complexity of the transport model utilized in the simulations. In general, the more accurate the transport model is, the greater the time reduction becomes. The number of species becomes especially critical for the multicomponent transport model, because it determines the dimension of the diffusion-velocity matrix that needs to be inverted. In that case, depending on pressure, temperature, and equivalence ratio the overall execution time associated with the reduced chemistry can be as much as an order of magnitude lower than that of the skeletal chemistry. In any case, as can be expected the fastest calculations are achieved when combining the 8-step reduced chemistry with the constant-Lewis-number transport model, a sufficiently accurate computational approach for many purposes, as indicated by our simulations.

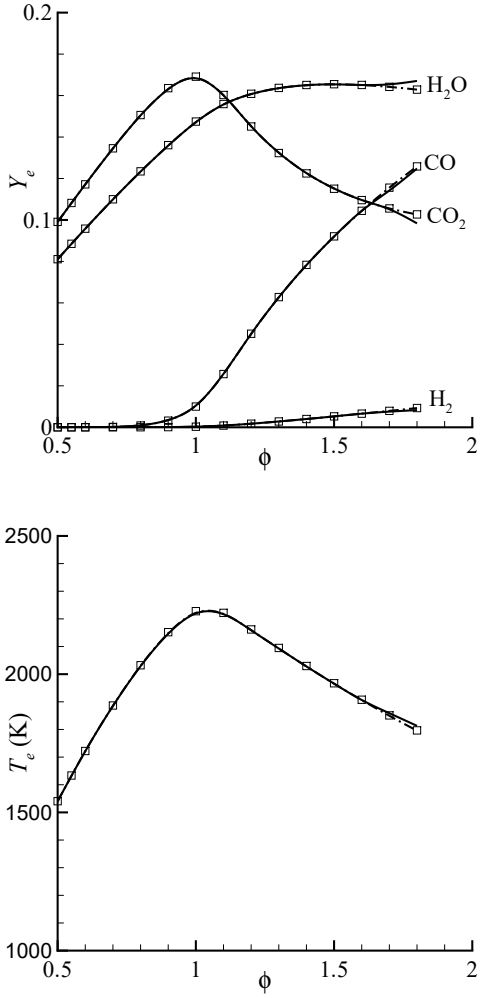

Figure 1.: The variation with equivalence ratio of the adiabatic flame temperature T_e and associated equilibrium mass fractions for a methanol-air mixture initially at normal atmospheric conditions as obtained with different chemistry descriptions (symbols: San Diego mechanism; solid curves: 38-step mechanism; dashed curves: 8-step reduced mechanism).

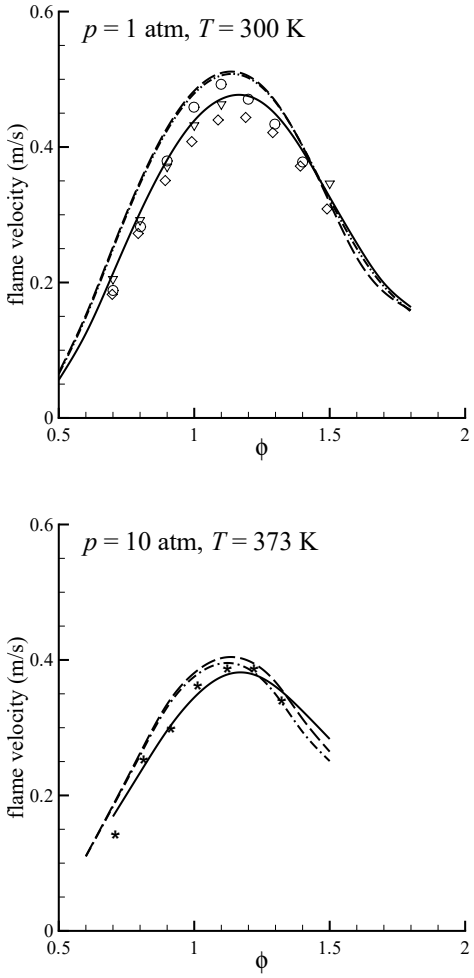

Figure 2.: Variation of the flame velocity with the equivalence ratio at 300 K for $p = 1$ atm (upper plot) and at 373 K for $p = 10$ atm (lower plot) computed with different chemistry descriptions (solid curves: San Diego mechanism; dashed curves: 38-step mechanism; dot-dashed curves: 8-step reduced mechanism) and measured experimentally ($\circ$ Saeed and Stone [46]; $\triangledown$ Vancoillie et al. [47]; $\lozenge$ Sileghem et al. [48]; $\star$ Beeckman et al. [49])

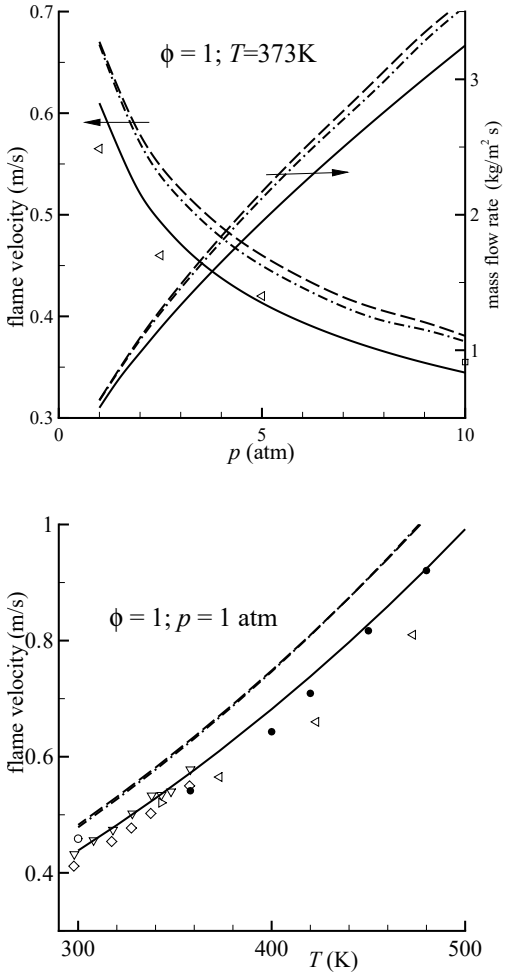

Figure 3.: The variation of the flame speed and mass flow rate of a stoichiometric methanol-air flame with the pressure (upper plot) and flame speed as a function of the initial gas temperature (lower plot) as obtained from numerical computations (solid curves: San Diego mechanism; dashed curves: 38-step mechanism; dot-dashed curves: 8-step reduced mechanism) and from flame velocity experimental measurements (○ Saeed and Stone [46]; ▽ Vancoillie et al [47]; ◊ Sileghem et al. [48]; □ Beeckman et al. [49]; ● Liao et al. [54]; ◁ Zhang et al. [55]; ▷ Veloo et al [56]).

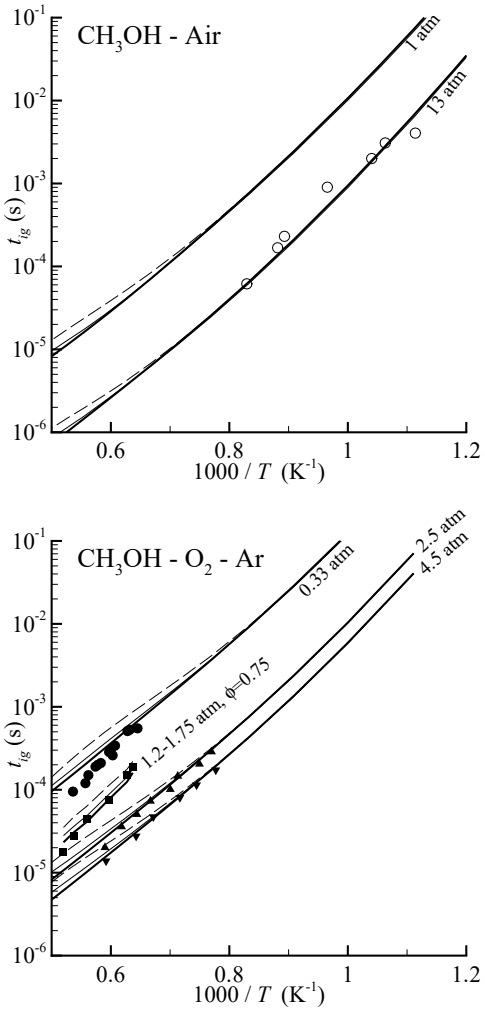

Figure 4.: The variation with the initial temperature of the induction time of methanol-air and methanol-O_2-Ar mixtures obtained from computations of homogeneous adiabatic ignition histories in an isochoric reactor with detailed (thick solid curves), skeletal (thin solid curves), and reduced (dashed curves) chemistry descriptions and from experimental measurements by Cooke et al. • [57] (stoichiometric mixture at $p = 0.33$), Bowman et al. ■ [58] (lean mixtures with equivalence ratio $\phi = 0.75$ at $p \in [1.2\ 1.75]$ atm), Natarajan et al. [59] (stoichiometric mixtures at $p = 2.5$ atm ▲ and at $p = 4.5$ atm ▼) and Fieweger et al. [60] ◯ (stoichiometric mixtures at $p = 13$ atm).

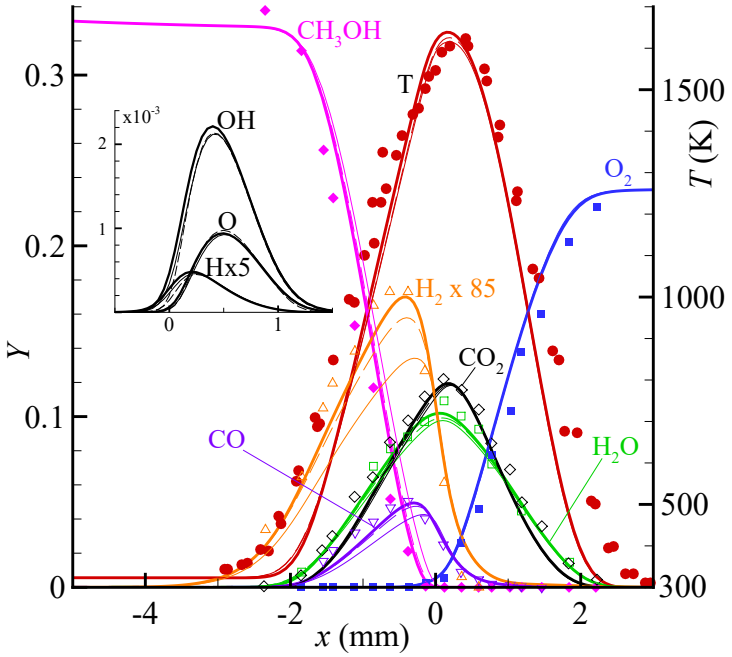

Figure 5.: Profiles of temperature and main-species mass fraction across a counter-flow diluted methanol-air diffusion flame with fuel mass fraction $Y_{\mathrm{CH_3OH}} = 0.329$, strain rate $A = 100\ \mathrm{s}^{-1}$, and fuel and air temperatures $T_1 = 323$ K and $T_2 = 298$ K as obtained from experimental measurements [62] (symbols) and from numerical computations with multicomponent transport including thermal diffusion (thick solid curves: 38-step skeletal mechanism; thin solid curves: 8-step reduced mechanism) and with constant Lewis numbers and a 38-step skeletal mechanism (dashed curves).

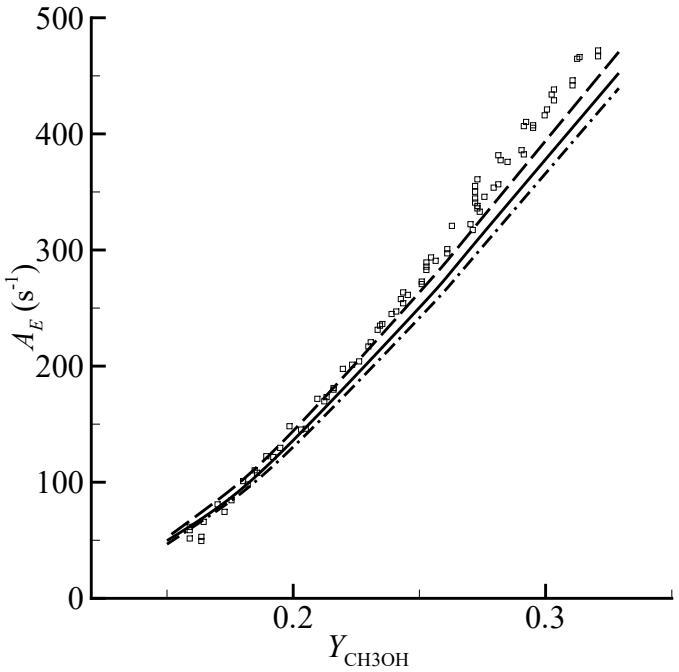

Figure 6.: Variation of the extinction strain rate A_E with the mass fraction of methanol Y_{CH_3OH} in its feed stream for methanol-air counterflow diffusion flame at atmospheric pressure with fuel-feed temperature $T_1 = 323$ K and air temperature $T_2 = 298$ K. The symbols are the experimental measurements by Seiser et al. [62], while the curves represent numerical results corresponding to the detailed mechanism (solid curves), to the 38-step skeletal mechanism (dashed curves), and to the 8-step reduced mechanism (dot-dashed curves) with a mixture-average model adopted in all cases for the transport description.

Table 1.: Rate coefficients in Arrhenius form $k = AT^n \exp\left[-E/(R^oT')\right]$ for the skeletal mechanism. Units are mol, s, cm^3, cal, and K.

No	Reaction		A^{a}	n	E^{a}
1	$H+O_2 \rightleftharpoons OH+O$		3.52×10^{16}	-0.70	17,069.79
2	$H_2+O \rightleftharpoons OH+H$		5.06×10^{4}	2.67	6,290.63
3	$H_2+OH \rightleftharpoons H_2O+H$		1.17×10^{9}	1.30	3,635.28
4	$H_2O+O \rightleftharpoons 2\ OH$		7.00×10^{5}	2.33	14,548.28
5	$H+O_2+M^{(1)} \rightleftharpoons HO_2+M^{(1)}$	k_0	5.75×10^{19}	-1.40	0.00
		k_∞	4.65×10^{12}	0.44	0.00
6	$H+OH+M^{(2)} \rightleftharpoons H_2O+M^{(2)}$		4.00×10^{22}	-2.00	0.00
7	$HO_2+H \rightleftharpoons 2\ OH$		7.08×10^{13}	0.00	294.93
8	$HO_2+H \rightarrow H_2+O_2$		1.66×10^{13}	0.00	822.90
9	$HO_2+H \rightleftharpoons H_2O+O$		3.10×10^{13}	0.00	1720.84
10	$HO_2+O \rightarrow OH+O_2$		2.00×10^{13}	0.00	0.00
11	$HO_2+OH \rightleftharpoons H_2O+O_2$		7.00×10^{12}	0.00	-1,092.96
			4.50×10^{14}	0.00	10,929.64
12	$H_2O_2+M^{(3)} \rightarrow 2\ OH+M^{(3)}$	k_0	7.60×10^{30}	-4.20	51,071.86
		k_∞	2.63×10^{19}	-1.27	51,071.86
13	$2\ HO_2 \rightarrow H_2O_2+O_2$		1.030×10^{14}	0.00	11042.07
			1.940×10^{11}	0.00	-1408.94
14	$CO+OH \rightleftharpoons CO_2+H$		4.40×10^{6}	1.50	-740.92
15	$HCO+M^{(4)} \rightarrow CO+H+M^{(4)}$		1.86×10^{17}	-1.00	17,000
16	$HCO+H \rightarrow CO+H_2$		5.00×10^{13}	0.00	0.00
17	$HCO+OH \rightarrow CO+H_2O$		3.00×10^{13}	0.00	0.00
18	$HCO+O_2 \rightarrow CO+HO_2$		7.58×10^{12}	0.00	409.89
19	$CH_2O+H \rightarrow HCO+H_2$		5.74×10^{7}	1.90	2,748.57
20	$CH_2O+O \rightarrow HCO+OH$		3.50×10^{13}	0.00	3,513.38
21	$CH_2O+OH \rightarrow HCO+H_2O$		3.90×10^{10}	0.89	406.31
22	$CH_2O+HO_2 \rightarrow HCO+H_2O_2$		4.11×10^{4}	2.50	10,210.33
23	$CH_4+H \rightleftharpoons H_2+CH_3$		1.30×10^{4}	3.00	8,037.76
24	$CH_3+O \rightarrow CH_2O+H$		8.43×10^{13}	0.00	0.00
25	$H+CH_3+M^{(5)} \rightarrow CH_4+M^{(5)}$	k_0	2.47×10^{33}	-4.76	2,440.01
		k_∞	1.27×10^{16}	-0.630	382.89
26	$CH_3O+O_2 \rightarrow CH_2O+HO_2$		4.28×10^{-13}	7.60	-3,537.28
27	$CH_3O+M^{(5)} \rightarrow CH_2O+H+M^{(5)}$		7.78×10^{13}	0.00	13,513.38
28	$CH_2OH+H \rightarrow CH_2O+H_2$		3.00×10^{13}	0.00	0.00
29	$CH_2OH+H \rightleftharpoons CH_3+OH$		2.50×10^{17}	-0.93	5,126.91
30	$CH_2OH+O_2 \rightarrow CH_2O+HO_2$		5.00×10^{12}	0.00	0.00
31	$CH_2OH+M^{(5)} \rightarrow CH_2O+H+M^{(5)}$		5.00×10^{13}	0.00	25,119.50
32	$CH_3O+M^{(5)} \rightleftharpoons CH_2OH+M^{(5)}$		1.00×10^{14}	0.00	19,120.46
33	$CH_3OH+OH \rightarrow CH_2OH+H_2O$		1.44×10^{6}	2.00	-838.91
34	$CH_3OH+OH \rightarrow CH_3O+H_2O$		4.40×10^{6}	2.00	1,505.74
35	$CH_3OH+H \rightarrow CH_2OH+H_2$		1.354×10^{3}	3.20	3,490.68
36	$CH_3OH+HO_2 \rightarrow CH_2OH+H_2O_2$		8.00×10^{13}	0.00	19,383.37
37	$CH_3OH+O_2 \rightarrow CH_2OH+HO_2$		2.00×10^{13}	0.00	44,933.08
38	$CH_3OH+M^{(5)} \rightarrow CH_3+OH+M^{(5)}$	k_0	2.95×10^{44}	-7.35	95,460
		k_∞	1.9×10^{16}	0.00	91,778

Chaperon efficiencies are:

[M1] = 0.70[Ar] + 0.70[He] + 2.50[H_2] + 16.00[H_2O] + 1.20[CO] + 2.40[CO_2] + 1.50[C_2H_6] + 1.00[other]

[M2] = 0.38[Ar] + 0.38[He] + 2.50[H_2] + 12.00[H_2O] + 1.90[CO] + 3.80[CO_2] + 1.00[other]

[M3] = 0.40[Ar] + 0.40[He] + 2.00[H_2] + 6.00[H_2O] + 1.50[CO] + 2.00[CO_2] + 2.00[CH_4] + 3.00[C_2H_6] + 1.00[other]

[M4] = 1.90[H_2] + 12.00[H_2O] + 2.50[CO] + 2.50[CO_2] + 1.00[other]

[M5] = 0.70[Ar] + 2.00[H_2] + 6.00[H_2O] + 1.50[CO] + 2.00[CO_2] + 2.00[CH_4] + 1.00[other]

Pressure dependent reactions are described by the TROE-formulation [41]. The centering parameters are given by:

$F_{c,5f} = 0.5$

$F_{c,12f} = 0.265\ \exp(-T/94\ K) + 0.735\ \exp(-T/1756\ K) + \exp(-5182\ K/T)$

$F_{c,25f} = 0.217\ \exp(-T/74\ K) + 0.783\ \exp(-T/2941\ K) + \exp(-6964\ K/T)$